AO16: Investigating the radiance emitted by the Earth using AATSR data

Candidate number: 469247
Supervisors: Dr R G Grainger and Dr G E Thomas
Word count: 5300

Abstract

The Earth's radiation budget at the top of the atmosphere is a balance of the incoming shortwave radiation from the sun, outgoing reflected shortwave radiation and longwave radiation emitted from the surface or the atmosphere exiting to space. The Advanced Along-Track Scanning Radiometer (AATSR) measures the reflectance of shortwave solar radiation and the brightness temperature corresponding to longwave radiation emitted from the Earth-atmosphere system as it orbits the Earth, covering most of the Earth's surface in a three day period.

Data from the radiometer for the period from August 2002 to February 2012 were used to calculate global means of the measured reflectances and brightness temperatures, which were then plotted as a time-series. The seasonal variation of the reflectances in the visible and near infra-red channels has a standard deviation of approximately 0.75 %, while the brightness temperatures in the thermal infra-red channels have a standard deviation of approximately 2.0 K during the day and 1.5 K during the night.

Correlations between the global means in the channels suggest that the observed reflectances and brightness temperatures are mainly due to cloud, and so any inter-annual variation would be due to changing amounts or thickness of cloud in the atmosphere.

To look for any inter-annual variation over the last ten years, the seasonality was removed by finding moving averages. The plots of these moving averages show some variation, with a range of approximately 1 % for the visible and near infra-red channels and 1 K for the thermal infra-red channels. By comparison with averaged reflectances and brightness temperatures over different land types (land, ocean and desert) it was found that, as the same pattern is not observed over each of the regions, the observed global pattern is due to something changing in our atmosphere (such as cloud amount or cloud thickness, or the Earth's radiating temperature), rather than the calibration of the instrument deteriorating over time which would affect all regions in the same way.

1 Introduction

1.1 Earth's Radiation Budget

The Earth's Radiation Budget at the top of the atmosphere is made up of three major terms. Shortwave solar radiation incident on the Earth, shortwave radiation reflected back to space by the Earth's surface or the atmosphere, and thermal infrared radiation emitted from the Earth's surface and atmosphere exiting to space. The Sun's outer layers are at a temperature of roughly 6000 K, whereas the Earth's effective radiating temperature is about 255 K [17]. Assuming both emit close to a blackbody, the blackbody spectra for these temperatures overlap very little, so that radiation from the Sun is at wavelengths less than 4 μm and radiation emitted by the Earth is at wavelengths longer than this. The net amount of radiation entering our atmosphere is given by [7]:

$$R_N(TOA) = (1/4)(S/a^2)(1-\alpha) - F_{LW}$$

where S is the total solar irradiance, a is the Earth-Sun distance in astronomical units, α is the albedo (fraction of incident solar radiation that is reflected back out to space) and F_{LW} is the longwave radiation flux exiting to space.

By looking at how the net amount of radiation exiting our atmosphere is changing over time, we can determine whether our Earth-atmopshere system is in equilibrium or not and whether the net energy flux is positive or negative. Any change in the Earth's radiation budget at the top of the atmosphere has a variety of possible causes - the incident solar radiation, or the planetary albedo of the Earth or the Earth's effective radiating temperature may be changing over time. Alternatively, the variation may be due to systematic errors from the instrument, although continuous on-board calibration should minimise these errors (see section 1.2). Random errors, such as instrumental noise, may get larger over time but the mean value should remain constant and so would not cause any variation.

There have been many satellite instruments used for investigating the terms of the radiation budget, such as ERBE (Earth's Radiation Budget Experiment), started in 1984 and CERES (Clouds and Earth's Radiant Energy System) which was first launched into space in December 1997. These are broad-band instruments in that they measure the radiances in a broad spectral width. AATSR is a narrow-band instrument, which measures the radiances in narrow channels at specific wavelengths. Using data from these satellite instruments, much research has been done into any long-term variations.

1.1.1 Incident solar radiation

Much of the energy entering our atmosphere is light from the Sun - about 99.7 % [17] - with the other 0.3 % coming from burning of fossil fuels, energy from radioactivity in the Earth and particles from space (mainly from the Sun). The solar constant is defined as the total solar irradiance at 1AU (mean Earth-Sun distance) and is roughly 1361 Wm^{-2}.

The value of total solar irradiance shows some variability with time [6] - an 11-year-cycle with peak-to-peak amplitude of about 0.1 % and some variation on a period of 27 days due to the Sun's rotation, with peak to peak amplitude of 0.2 %. If we take the total solar radiation to be about 1361 Wm^{-2}, these variations correspond to 1-3 Wm^{-2}.

1.1.2 Reflected solar radiation

There have been many studies that investigate how the Earth's albedo has changed over time. Palle et al (2009) [13] compared reflectances from measurements of earthshine, CERES and flux data from the International Satellite Cloud Climatology Project (ISCCP) from 1999 to 2007. When looking only at earthshine and ISCCP data, they found a weak increase in albedo in the period 1999-2003 and then a fairly constant albedo up until 2007. However, when CERES data was included in the comparison, they could find no trend in the Earth's albedo over the period of interest.

Kato (2009) [8] found little interannual variation in CERES data from March 2000 to February 2004 - the annual global mean TOA reflected shortwave irradiance for this period was 97.0 Wm^{-2} with a range of 96.8 to 97.2 Wm^{-2} (0.4 % of the mean value). Similarly, the annual global mean TOA longwave irradiance is 239 Wm^{-2} with a range between maximum and minimum of 0.1 % of this mean.

1.1.3 Outgoing longwave radiation

As well absorbing solar radiation, the Earth's surface and the atmosphere also emit radiation but at longer wavelengths.

Kandel and Viollier (2010) [7] analysed data from the Clouds and Earth's Radiant Energy System (CERES) and found that the change in the outgoing longwave flux is balanced by the change in the reflected shortwave radiation. They also found a well-defined annual cycle for the TOA net radiation, with net radiation exiting to space in July and entering our atmosphere in January.

1.2 The AATSR Instrument [2]

The Advanced Along Track Scanning Radiometer (AATSR) is the third in a series of ATSR instruments. ATSR-1 was launched on board ESA-1 in 1990, ATSR-2 was launched on board ESA-2 in 1995 and AATSR was launched on board ENVISAT in 2002. The satellites follow a sun-synchronous polar orbit around the Earth, so that it ascends or descends over each point on the Earth's surface at the same local time. For the descending node (when the satellite is moving from North to South), the satellite crosses

the equator with a local time of 10am. Each orbit has a period of about 100 minutes which means there is an average of fourteen orbits in one day. In a three-day period, the radiometer will have scanned almost every point on the Earth's surface. If only daytime or nighttime points are used, then the coverage is not quite global - latitudes close to one of the poles will be missing depending on the time of the year. The satellite has a repeat cycle of 35 or 165 days (the first orbit on the first day will be exactly aligned with the first orbit on the 35th or 165th day).

The scanning radiometer measures the incoming radiances and converts this signal into a reflectance for the visible or near infra-red channels, or a brightness temperature for the thermal infra-red channels. As well as measuring radiation from the surface and the atmosphere, the satellite also measures incident solar radiation once per orbit, and gives reflectances for these channels as a percentage using [16]:

$$r_{scene} = \frac{\pi L_{scene}}{E_{0,\lambda}}$$

where L_{scene} is the measured radiance and $E_{0,\lambda}$ is the spectral solar irradiance. The brightness temperature is the temperature a black-body (a black-body absorbs all incident radiation) would need to have in order to emit the measured radiation at that wavelength. It can be found from Planck's function [9]:

$$B_\lambda(T) = \frac{2hc^2}{\lambda^5(e^{hc/k_B\lambda T} - 1)}$$

where λ is the wavelength under consideration, B is the energy per unit area per unit time per unit solid angle per unit frequency and T is the brightness temperature.

There are three thermal infrared channels at wavelengths of 3.7, 11 and 12 μm. These channels were included on the instrument to determine the sea-surface temperature - 11 and 12 during both day and night, and 3.7 used mainly only during the night. However, they are also used to measure the temperature of land. A near infra-red wavelength at 1.6 μm is used for cloud clearing. ATSR-2 and AATSR have three additional visible channels at wavelengths of 0.55, 0.67 and 0.87 μm. The channels at 0.67 and 0.87 μm are used to study the amount of vegetation, as vegetation has a low reflectance at 0.67 μm but a high reflectance at 0.87 μm. The channel at 0.55 μm is at the green part of the visible spectrum, so the radiance in this channel gives information about the quality of vegetation. The wavelengths and primary purposes of the channels are summarised in table 1. While the ATSR series was designed to measure the sea surface temperature, the instruments have also been used to study other things such as global fire count trends [1].

Table 1: Summary of the narrowband channels on AATSR, with their primary purpose.

Channel	Wavelength	Primary purpose
Channel 1	0.55 μm	Vegetation
Channel 2	0.67 μm	Vegetation
Channel 3	0.87 μm	Vegetation
Channel 4	1.6 μm	Cloud clearing
Channel 5	3.7 μm	Sea surface temp.
Channel 6	11 μm	Sea surface temp.
Channel 7	12 μm	Sea surface temp.

In each scan, the radiometer scans a 512 km wide swath in the nadir direction (directly below the satellite) and then scans a swath at an angle of 55° along the track of the satellite. About 150 seconds later (when the satellite has moved approximately 1000 km along the track), the satellite passes over this point and takes a nadir measurement. This means that every point on the surface of the Earth has two measurements with two different optical path lengths. The nadir point of the satellite moves forward by 1 km during each scan. The radiometer performs on average 6.6 scans per second.

Before launch, calibration was done for all the channels - for the thermal infra-red channels, this included looking at a range of temperatures from 210 K to 315 K and checking for non-linearity in the detector response over this range [16]. During operation, continuous on-board calibration of the channels is performed [15]. For the thermal infra-red channels, there are two black-bodies on board at different temperatures (one at approximately 265 K and the other at 305 K). They are both viewed during every scan and are used to continuously calibrate the thermal channels by finding the gain, G and the offset O, so that a measured signal, C_{scene}, can be calculated from

the incoming radiance, L_{scene} by [15]:

$$C_{scene} = GL_{scene} + O$$

The visible and near infra-red channels are calibrated in a similar way using VISCAL, which is also scanned during every scan. The reflectance of the scene, r_{scene} is given by [16]:

$$r_{scene} = r_{viscal} \frac{C_{scene} - C_{dark}}{C_{VISCAL} - C_{dark}}$$

where C_{scene} is the signal count from the surface, C_{dark} is the signal count from the cooler blackbody and C_{VISCAL} is the signal count from the incident solar irradiance.

The calibration has been checked while in operation by looking at certain regions and comparing measurements from AATSR with other measurements, such as sea surface temperature from buoys in the ocean [15].

1.3 Level 1B data [2]

The level 1B data contains the top of the atmosphere reflectances (for the four visible and near infra-red channels) and brightness temperatures (for the thermal infrared channels) for both nadir and forward views on a rectangular grid with a resolution of 1km. It also contains flags for cloud and land identification and confidence flags for each pixel.

Because the radiometer scans a circular swath during each cycle, each pixel scanned by the instrument is moved to the nearest grid point. For parts of the scan, there are not enough measured pixels to fill the rectangular grid, and so a cosmetic fill is done, where the data for a missing pixel is inferred from the surrounding pixels. In this case, the confidence flag for that pixel will show that this has happened. Each across-track swath has a Julian time associated with it - this is the time that the across-track scan crosses the centre of the track. For the forward pixels, this time is the associated time for the nadir swath of the scan.

Clouds play a large role in the amount of radiation exiting to space, as they reflect more shortwave solar radiation back to space and block longwave radiation from the surface or atmosphere from exiting to space. In this project, data points that are cloudy and not cloudy are all included and so any variation found may be due to changing amounts of cloud in our atmosphere.

The scanning radiometers used to gather data (such as CERES, AATSR) capture instantaneous radiances from a particular direction in either a narrow band or a broad band. However, the reflected shortwave and emitted longwave radiation are usually reflected or emitted anisotropically. Much research has been done developing angular distribution models in order to convert these directional measurements to a hemispherical irradiance (see Loeb et al, 2002 [10]). Over vegetation it is found that the emitted longwave radiation is anisotropic [12]. The temperature obtained from a directional measurement may not give the true temperature of that surface. Otterman et al found that the viewing zenith angle that gave the least error was about 50°. From a nadir measurement, the hemispheric emission may have an error of about 10% [12]. In this project, instantaneous narrowband radiances from the AATSR satellite, both longwave and shortwave, are used to create a time-series of global and regional means of these radiances without converting them to top-of-the-atmosphere fluxes.

Clerbaux et al (2003) [3] found an anisotropy in the measured radiances in satellite data, depending on the azimuthal viewing angle - whether the point is viewed from the north or from the south affects what is measured. However, in this project, the top of the atmosphere reflectances and brightness temperatures are not calculated from hemispheric irradiances - instead, looking for a variation over time rather than actual values for the reflectance or temperature of the Earth.

2 Method

The level 1B dataset contains, for each 1km by 1km pixel, a measured reflectance (as a percentage of incident solar radiation) or brightness temperature (in Kelvin). It takes the satellite three days, with approximately fourteen orbits per day, to get near global coverage. Due to the inclination of the orbit, the instrument misses the poles and samples points near the poles more often than points at the equator, since the orbits overlap at higher altitudes. In order to compensate for this, a sinusoidal grid of the Earth's

surface was used, such that the Earth is divided into 2675 boxes of equal area. At the equator, a box corresponds to $4^\circ \times 4^\circ$ in latitude-longitude. For each box, a three-day mean reflectance or brightness temperature was found for each channel using data from the first nine days of each month from August 2002 to February 2012. As a result, each month has three means per box.

For the visible and near infra-red channels, only the daytime points (where the solar zenith angle is less than 90°) were used in the means. This was done because it was found that at night, the signal in these channels drops very close to zero, probably due to instrument noise rather than a climate effect. For the thermal channels, the daytime and nighttime points were averaged separately in order to avoid loss of generality.

Not all of the boxes have an average associated with them in every three-day period, mainly due to missing data from the satellite. The visible and near infra-red channels sometimes get saturated when the incoming radiance is too high - in this case the reflectance is given as zero. If one of these channels has missing data but non-zero data is present in the other visible channels, then it is assumed that this missing point is due to saturation and so it is replaced with the maximum value observed in that channel and included in the mean for that box.

A global mean was found by taking an unweighted average (so that each point of the Earth's surface has an equal weighting) over all boxes for each 3-day period. These global means are plotted in figure 1. Global means are only plotted if more than 2000 of the boxes (about 75% global coverage) contained data. It was found that global means with worse global coverage were generally anomalous. Because of the large number of data points (N) that go into each global average, the standard error (given by $\delta/\sqrt{N}$, where δ is the standard deviation) for these averages is very small and so errors have not been drawn on the plot. Outliers are marked in red. The mean and standard deviations of these global reflectances and brightness temperatures for each channel over the 10 year period were calculated.

Correlations between the global means in different channels were calculated using Pearson's product-moment correlation coefficient, $\rho_{X,Y}$, given by:

$$\rho_{X,Y} = \frac{E[(X-\mu_X)(Y-\mu_Y)]}{\sigma_X \sigma_Y}$$

This correlation coefficient looks for linear correlation between the two variables, X and Y. Perfect positive correlation has a coefficient of 1, while perfect negative correlation has a coefficient of -1. A coefficient close to zero implies no correlation.

To look for any inter-annual variability in the channels, moving averages were calculated by averaging over a subset of a year of global means and shifting this subset on by one data point each time. This removes the seasonal variation. These moving averages are plotted in figure 6.

In order to try to find a cause for any inter-annual variability found, means over certain regions with different land types were calculated to see whether the same variability would be observed regionally as well as globally. The latitude/longitude box over the Sahara desert ran from 10°W to 35°E and 15°N to 30°N. To look at land, an area in Asia (40°E to 120°E and 40°N to 60°N) was chosen. Over land, the visible channels respond to the amount and quality of vegetation if no cloud is present. In order to look at the reflectance and brightness temperature over sea, a region of the Pacific ocean (180°W to 120°W and 40°S to 40°N) was used.

Note that although the satellite measures radiances in two directions, nadir and forward (along-track), only plots of the nadir view are shown. During the analysis, it was found that while the reflectances and brightness temperatures were higher or lower for the different views (due to differing optical path lengths), the time-series looked the same. As a result, in what follows, only the nadir view plots have been included.

3 Results

The plots in figure 1 show the global mean reflectances for the four visible and near infra-red channels and the global mean brightness temperatures for the three thermal infra-red channels for day and night separately. The random error on these averages is small (due to the large number of data points) and so they are not drawn on the plot. The time series

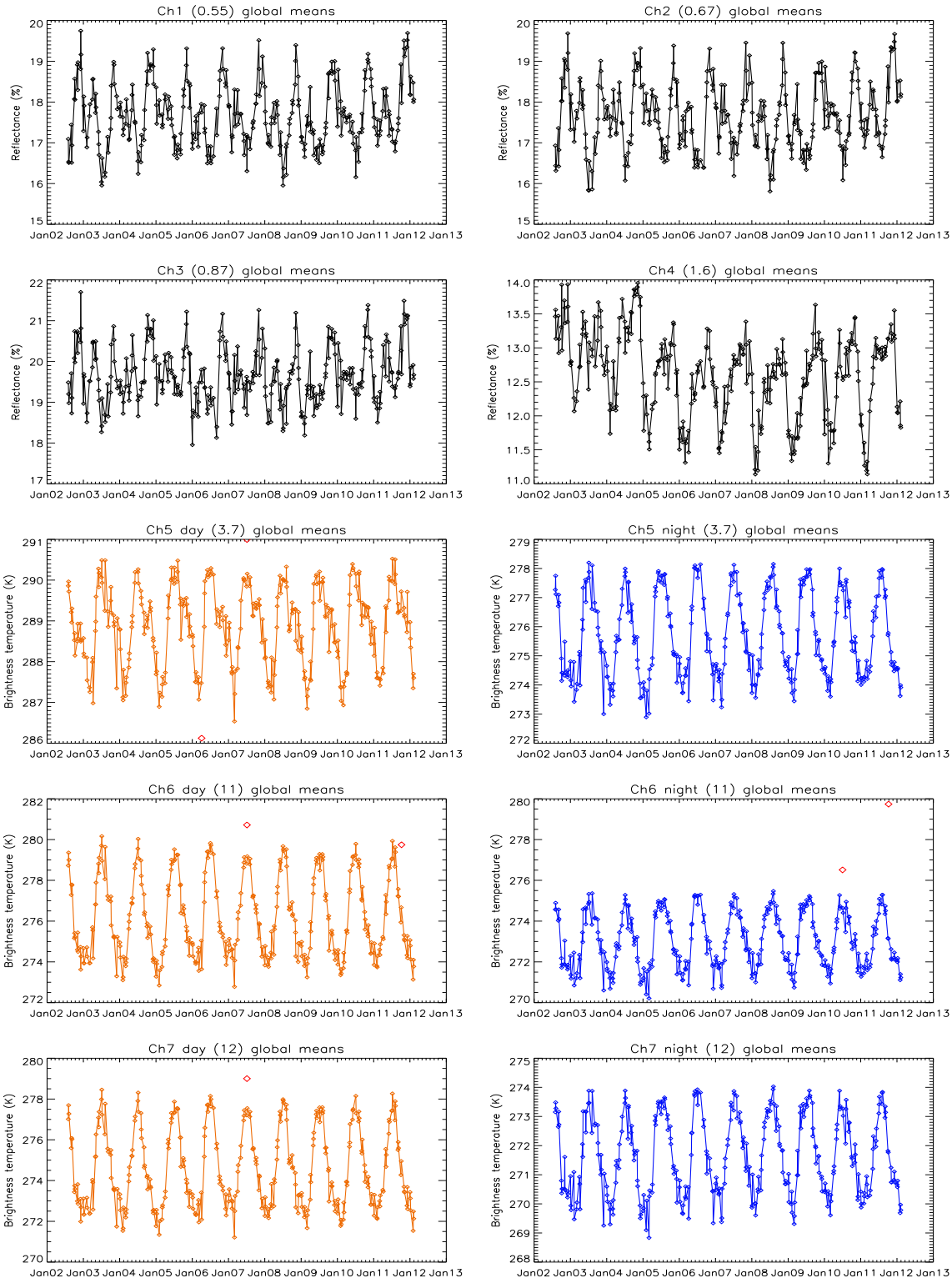

Figure 1: Time-series of 3-day global means for the first nine days in each month, from August 2002 to February 2012. The number in the title gives the wavelength for that channel in microns. The top four images are for the visible and near infra-red channels. The orange images are the thermal infra-red channels during the day, and the blue images are the thermal infra-red channels during the night

for the thermal infra-red channels show the variation due to the seasons - maxima in brightness temperature occur in July and minima occur in January. This seasonal variation appears in the global mean brightness temperature because most of the land is in the Northern hemisphere, where winter occurs around January and summer occurs around July. Fasullo and Trenberth (2008) [5] also found the global variation in outgoing longwave radiation matches the variation in land surface temperature. Land responds more quickly to changes in incident radiation than the oceans, which has large inertia to changes in temperature.

Figure 2 shows these time series for channel 1 over different regions. The top left plot is of the global mean reflectance. The other plots are for the Sahara (orange), Asia (green) and the Pacific Ocean (blue). The individual regions have greater variability - the ranges for the Sahara, Asia and the Pacific are roughly 10 %, 20 % and 6 % respectively. In comparison, the range of the global mean reflectance is about 3 % - this shows that large regional variability cancels out to give small global variability, similar to findings of Kato (2009) [8].

The visible and near infra-red channels, at 0.55 μm, 0.67 μm, 0.87 μm and 1.6 μm each have an average reflectance and standard deviation between August 2002 and February 2012 of $17.68\% \pm 0.78$, $17.66\% \pm 0.82$, $19.66\% \pm 0.71$ and $12.60\% \pm 0.64$ respectively. In channel 4 (1.6 μm), it is clear to see a decrease in this channel since 2002.

The reflectances in channel 1 and channel 2 have a strong positive correlation, with Pearson's coefficient of product-moment correlation equal to 0.985 (see figure 3). The correlation between channel 1 and channel 3 is still positive, but not as strong (0.905). On the other hand, channel 4 has very weak correlation with each of the visible channels (0.366, 0.326 and 0.598 for channels 1, 2 and 3 respectively).

Channels 2 and 3 were primarily intended to study vegetation - channel 2 has a low reflectance over vegetation while channel 3 has a high reflectance. As a result, these channels should show a negative correlation over vegetation. Globally, these channels show a positive correlation, with a correlation coefficient of 0.904 (see figure 3). Over Asia, the correlation coefficient is 0.921. As the correlation is positive and strong over land, this suggests that the measured reflectances are primarily due to reflectances from clouds or the atmosphere rather than the surface. Cloud has a high reflectance for all shortwave radiation and so all of the shortwave channels will have a positive correlation. Kato (2009) [8] found that clouds were mainly responsible for increased

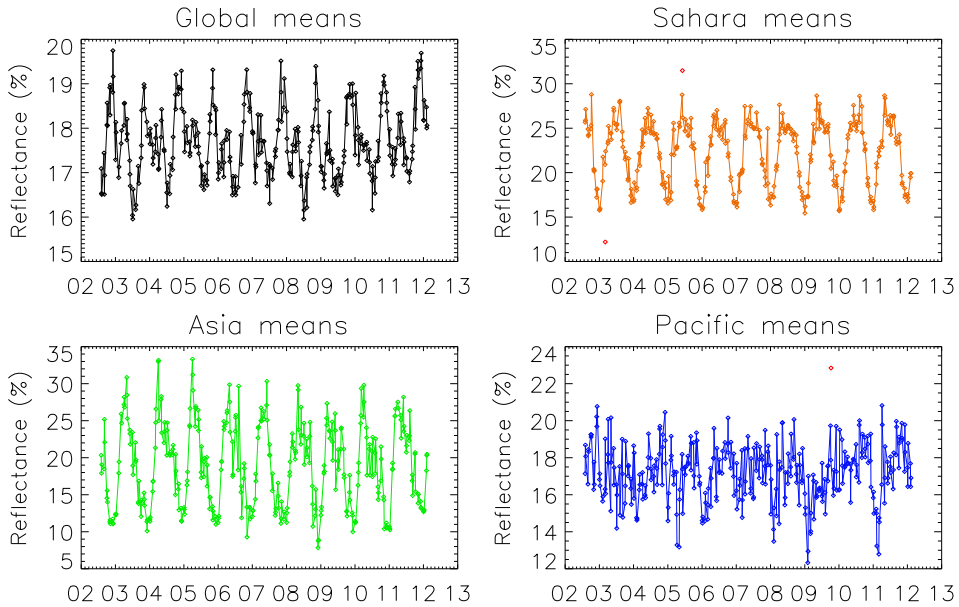

Figure 2: Time series for channel 1 (0.55 μm) - globally (black), over the Sahara (orange), over Asia (green) and over the Pacific ocean (blue).

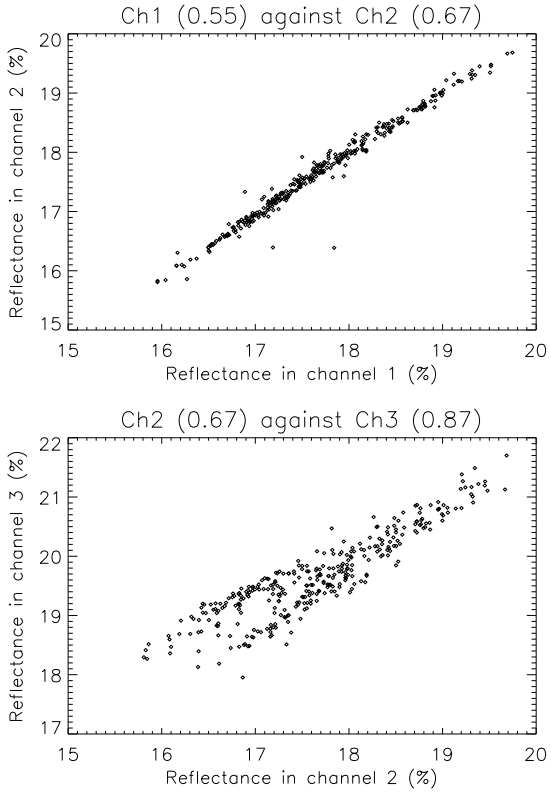

Figure 3: Scatter plots of the global mean reflectances for channel 1 (0.55 μm) against channel 2 (0.67 μm) (top) and channel 2 (0.67 μm) against channel 3 (0.87 μm) (bottom). The Pearson's coefficients of correlation are 0.985 and 0.904 respectively.

variability of reflected shortwave and longwave radiance at the top of the atmosphere by comparing clear-sky measurements with all-sky measurements.

The thermal IR channels, at 3.7 μm, 11 μm and 12 μm, have an average brightness temperature and standard deviation of $288.9\,\mathrm{K} \pm 1.0$, $276.2\,\mathrm{K} \pm 2.0$ and $274.6\,\mathrm{K} \pm 1.9$ during the day. During the night, these brightness temperatures drop to $275.7\,\mathrm{K} \pm 1.4$, $273.0\,\mathrm{K} \pm 1.4$ and $271.6\,\mathrm{K} \pm 1.4$. The last two channels are used to retrieve surface temperatures during the day and night, while the channel at 3.7 μm is used primarily at night to retrieve surface temperatures. During the day, this channel picks up reflected solar radiation which explains why its daytime mean value is much higher than its nighttime mean value. For channels 6 and 7, the difference between the mean daytime and nighttime temperatures is only 3 K, whereas for channel 5, this difference is 14 K. Also, the correlation coefficients between day and night global means for channel 5 is weaker than the correlations between day and night for channels 6 and 7 (0.859, 0.947 and 0.947 between day and nighttime means for channels 5, 6 and 7 respectively).

The mean surface temperature of the Earth is 288 K and the effective radiating temperature of the Earth-atmosphere system is 254 K [9]. The observed mean brightness temperatures in channels 6 and 7 fall between these two temperatures. Cloud is opaque to longwave radiation from the Earth's surface and the cloud tops are at a lower temperature, and so over cloudy areas, a lower brightness temperature is observed than the surface temperature. The channels on AATSR are designed to be window channels, in that little radiation at these wavelengths is absorbed or scattered by gases in the atmosphere and so the signal is dominated by either the surface or clouds. Because the global means combine cloudy measurements with clear-sky measurements, it is found that the brightness temperature is lower than the surface temperature, but higher than the effective radiating temperature. Channel 6 is slightly higher than channel 7 because channel 7 is slightly more sensitive to water vapour and so measurements from the lower atmosphere are included in the global means. The lower atmosphere is at a lower temperature, and so we measure a lower brightness temperature for this channel.

Daytime means for channels 6 and 7 are very strongly positively correlated (figure 4), with a correlation coefficient of 0.997. Channel 5 is more weakly correlated with channels 6 and 7 during the day (0.876 and 0.875 respectively) as expected, as this channel picks up reflected solar radiation as well as emitted terrestrial radiation during the day.

In the presence of clouds, more shortwave solar radiation is reflected. Longwave radiation from the Earth's surface and lower atmosphere are blocked by the clouds, and so the brightness temperature of the top of the clouds and upper atmosphere is observed. Figure 5 shows the correlation between shortwave global mean reflectance (channel 1) and longwave global mean brightness temperature (channel 6). These channels show a negative correlation, although it is weak (the correlation coefficient is -0.573). This weak negative correlation is present whenever channels 1, 2 and 3 are plotted against

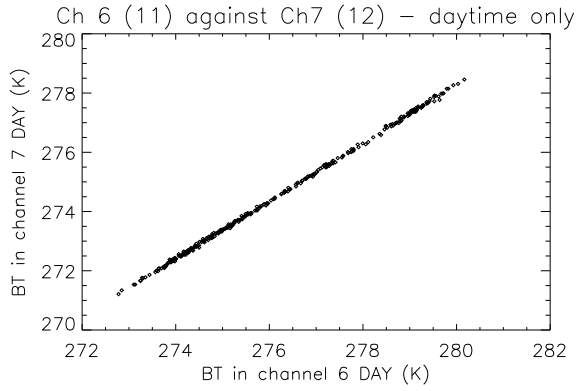

Figure 4: The global mean brightness temperatures in channel 6 (11 μm) plotted against those in channel 7 (12 μm). The Pearson's coefficient of correlation is 0.997.

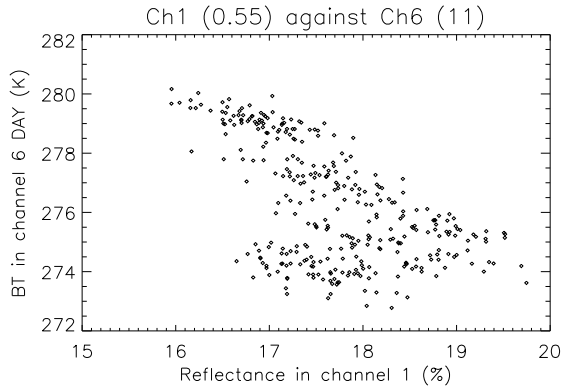

Figure 5: The global mean reflectance in channel 1 (0.55 μm plotted against global mean brightness temperature in channel 6 (11 μm). The Pearson's coefficient of correlation is -0.573.

channels 5, 6 and 7. Channel 4, on the other hand, shows very little correlation with channels 6 and 7. This implies that most of the signal is due to reflection and emission from clouds.

In order to determine how the measured reflectances and brightness temperatures in each channel have changed over the last ten years, a moving average was calculated (by taking the mean of a subset of a year). Global and regional moving averages for all of the visible and near infra-red channels are plotted in figure 6. The global moving averages for the visible and near infra-red channels show some variation, with standard deviations of 0.134 % in channel 1, 0.144 % in channel 2, 0.166 % in channel 3 and 0.250 in channel 4.

Loeb et al (2007) [11] compared global top-of-the-atmosphere shortwave radiances from earthshine observations and data from CERES, MODIS and ISCCP, in the period from 2000 and 2005. A plot of deseasonalized anomalies (the difference between the average in a given month and the average of the same month over all years in the period of interest) of shortwave radiation for land and oceans show a downward trend from 2002 to 2004, before flattening out. This matches the variation found for all of the visible channels (figure 6) - at the beginning of the AATSR data (2002), the global moving averages are decreasing. However, the reflectances at these wavelengths started to increase again in 2004, unlike the findings of Loeb et al [11].

Cloud is an important factor affecting the reflectance. Looking at cloud data from the International Satellite Cloud Climatology Project (ISCCP), Evan et al (2007) [4] have found a variation in the cloud amount, in the period from mid-2002 to 2005 that matches the variation in the global moving averages found in the visible channels (see figure 6) - an initial decrease followed by an increase. This suggests that the changes in reflectance are due to changing amounts or thickness of cloud.

Moving averages for the thermal infra-red channels (for day and night separately) are also plotted in figure 6. They all show a similar inter-annual variation, with a range between minima and maxima of roughly 1 K. The standard deviations for channels 5, 6 and 7 during the day are 0.079, 0.107 and 0.103 respectively.

In addition to global moving averages, moving averages over certain regions are also plotted. Looking at channel 1 only, the standard deviations for these regional moving averages are 0.210 %, 0.576 % and 0.360 % for the Sahara, Asia and the Pacific respectively. In comparison, the global moving average for channel 1 has a standard deviation of 0.134 % - approximately half the regional deviations. This supports the previous finding that small regions have large variability but that this variability cancels out when a global mean is calculated.

The global inter-annual variation in each channel isn't repeated in the regional moving averages, which suggests that the observed variations are primarily due to a change in the atmosphere that is affected by different land types, as opposed to a systematic error

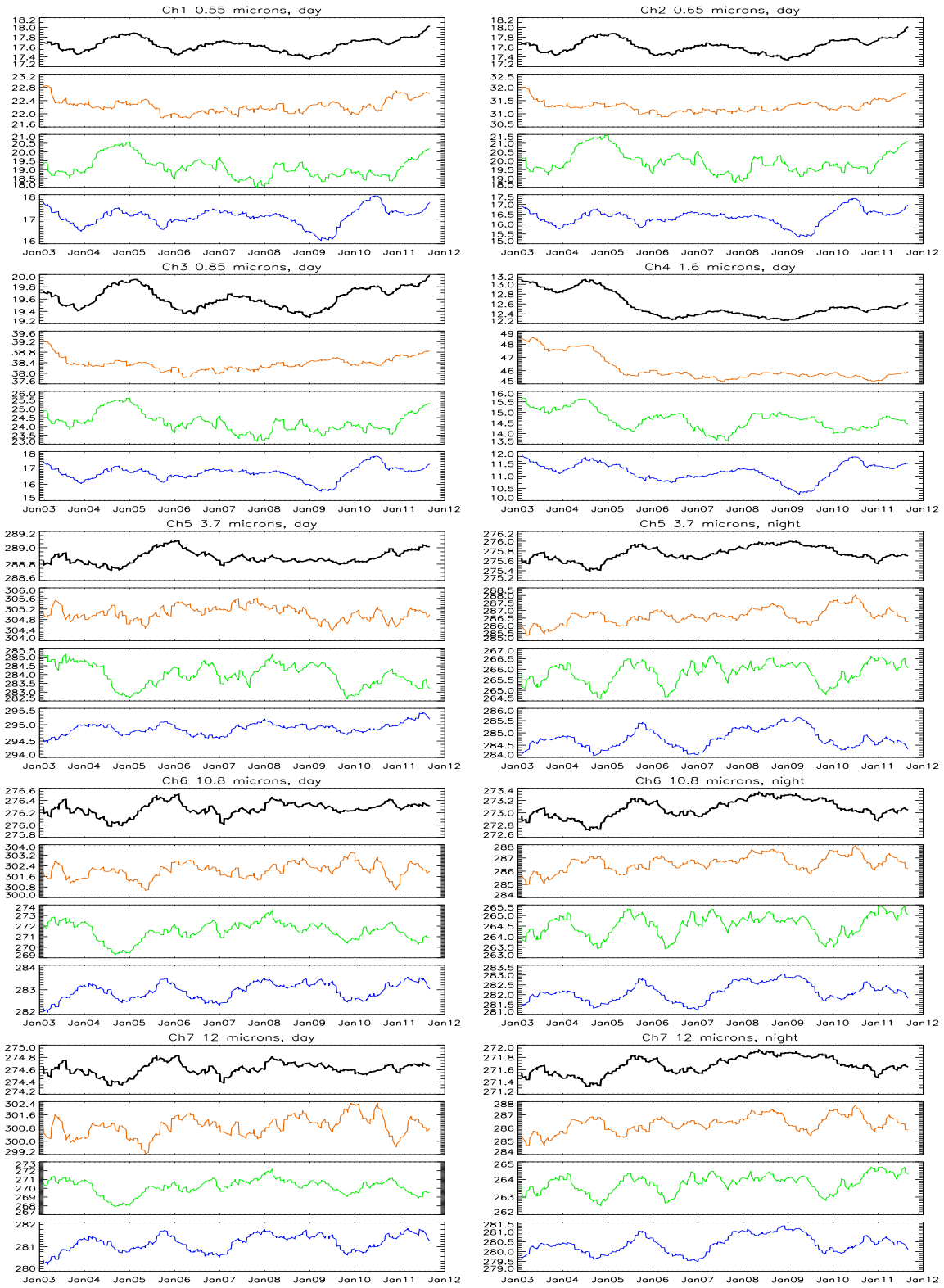

Figure 6: Moving averages for each channel. Each data point is a mean over one year, plotted against the middle of that year. Shown are the trends of the global means (black line), and over specific regions - Sahara (orange line), Asia (green line) and the Pacific Ocean (blue line)

from the calibration of the instrument. Any systematic error would be present for all regions.

4 Conclusions

The AATSR instrument on ESA's ENVISAT satellite measures reflectances and brightness temperatures in seven narrow bands centred around certain wavelengths. The instrument samples most of the Earth's surface along two different directions in a three-day period and has been running since August 2002. For each channel, time series of global mean reflectances and brightness temperatures have been produced. It is found that the global mean brightness temperatures exhibit a seasonal variation corresponding to the seasons experienced by the Northern hemisphere (where most of the land is found). This is due to the quicker response of land to changes in temperature than the ocean.

Correlations between channels were found in order to determine whether the observed reflectances and brightness temperatures are dominated by surface measurements or cloud measurements. Strong positive correlation between all of the visible channels (the correlation coefficients are all at least 0.8) suggests that most of the signal is from clouds in the atmosphere, as they reflect shortwave radiation. Over vegetation, channel 2 and 3 should have a low/high reflectance respectively, and a negative correlation between these channels would be observed. Looking at dat over Asia, the correlation os still positive (Pearson's coefficient of correlation is 0.921). The weak, negative correlation between channel 1 (shortwave) and channel 6 (longwave) has a coefficient of -0.573 which further implies that cloud is dominating the measured signal, as clouds reflect shortwave radiation and block longwave radiation.

In order to look for any inter-annual variation in the channels, moving averages were calculated by averaging a year of global means at a time. These plots show some small variation globally. In the visible and near-IR channels, this global trend involves minima and maxima, with a period of roughly 2.5 years. The standard deviations tell us about the variability - for channels 1, 2, 3 and 4, the standard deviations in the reflectances for this inter-annual global variability are 0.134 %, 0.144 %, 0.166 % and 0.250 % respectively. For the thermal channels, there is a global variability that shows in all three channels, both during the day and during the night. The global standard deviations for the daytime thermal trends are 0.079 K, 0.107 K and 0.103 K. During the night, the global standard deviations are 0.142 K, 0.147 K and 0.144 K. The correlations between channels suggest that the signal is dominated by cloud measurements and so this variation is due to changes in cloud amount or thickness in the atmosphere.

Moving averages for certain regions were found in the same way as the global moving averages (the Sahara, Asia and the Pacific as examples of desert, land and ocean). The variation observed in the global moving averages is not present over all regions, which suggests that it is due to changes in the atmosphere - either the albedo of the earth or the temperature leading to more or less emitted longwave radiation - rather than changes in the instrument calibration.

Future work on this time series should include analysis of all of the AATSR data (due to time restrictions, only the first nine days of each month have been included in this analysis). In addition, data from ATSR-1 and ATSR-2 should be analysed in a similar way to see whether any long-term variability is repeated. ATSR-1 was launched in 1991 and ATSR-2 was launched in 1995 (the three visible channels for vegetation monitoring were introduced on ATSR-2). Using this data would significantly extend the period of the time series.

To further determine whether the signal is dominated by cloud, it would be interesting to compare the global mean reflectances and brightness temperatures from AATSR with other datasets, such as the ISCCP (International Satellite Cloud Climatology Project) [14], which looks at data from several instruments to determine the amount of cloud in the atmosphere as well as type and optical thickness.

The results presented here, showing small inter-annual variability, have been found using a well-calibrated instrument. As such, they could be used to test the accuracy of climate models in predicting the reflectances and brightness temperatures at the top of the atmosphere. This could be done by sampling from the model as if AATSR were orbiting it and comparing these observations with the actual measurements from AATSR.

References

[1] O. Arino, S. Casadio, and D. Serpe. Global night-time fire season timing and fire count trends using the ATSR instrument series. *Remote Sensing of Environment*, 116:226–238, 2012.

[2] A. Birks. European Space Agency - EnviSat AATSR Product Handbook, September 2004. Issue 1.2.

[3] N. Clerbaux, A. Ipe, C. Bertrand, S. Dewitte, B. Nicula, and L. Gonzalez. Evidence of azimuthal anisotropy for the thermal infrared radiation leaving the Earth's atmosphere. *International Journal of Remote Sensing*, 24(14):3005–3010, 2003.

[4] A. T. Evan, A. K. Heidinger, and D. J. Vimont. Arguments against a physical long-term trend in global ISCCP cloud amounts. *Geophysical Research Letters*, 34:L04701, 2007.

[5] J. T. Fasullo and K. E. Trenberth. The Annual Cycle of the Energy Budget. Part I: Global Mean and Land-Ocean Exchanges. *Journal of Climate*, 21:2297–2313, 2008.

[6] C. Froehlich and J. Lean. Solar radiative output and its variability: evidence and mechanisms. *The Astronomical Astrophysics Review*, 12(4):273, 2004.

[7] R. Kandel and M. Viollier. Observation of the Earth's radiation budget from space. *Comptes Rendus Geoscience*, 342(4):286–300, 2010.

[8] S. Kato. Interannual variability. *Journal of Climate*, 22(18):4893–4907, 2009.

[9] K. N. Liou. *An Introduction to Atmospheric Radiation*. Academic Press, 2nd edition, 2002.

[10] N. G. Loeb, N. Manalo-Smith, S. Kato, W. F. Miller, S. K. Gupta, P. Minnis, and B. A. Wielicki. Angular Distribution Models for Top-of-Atmosphere Radiative flux Estimation from the Clouds and the Earth's Radiant Energy System Instrument on the Tropical Rainfall Measuring Mission Satellite. Part I: Methodology. *Journal of Applied Meteorology*, 42(2):240–265, 2003.

[11] N. G. Loeb, B. A. Wielicki, F. G. Rose, and D. R. Doelling. Variability in global top-of-atmosphere shortwave radiation between 2000 and 2005. *Geophysical Research Letters*, 34:L03704, 2007.

[12] J. Otterman, J. Susskind, T. Brake, D. Kimes, R. Pielke, and T. J. Lee. Inferring the thermal-infrared hemispheric emission from a sparsely-vegetated surface by directional measurements. *Boundary-Layer Meteorology*, 74:163–180, 1995.

[13] E. Palle, P. R. Goode, and P. Montanes-Rodriguez. Interannual variations in Earth's reflectance 1999-2007. *Journal of Geophysical Research*, 114:D00D03, 2009.

[14] W. B. Rossow and R. A. Schiffer. ISCCP Cloud Data Products. *Bulletin of the American Meteorological Society*, 72(1):2–20, 1991.

[15] D. Smith, C. Mutlow, J. Delderfield, B. Watkins, and G. Mason. ATSR infrared radiometric calibration and in-orbit performance. *Remote Sensing of Environment*, 116:4–16, 2012.

[16] D. L. Smith, J. Delderfield, D. Drummond, T. Edwards, C. T. Mutlow, P. D. Read, and G. M. Toplis. Calibration of the AATSR instrument. *Advanced Space Research*, 28(1):31–39, 2001.

[17] F. W. Taylor. *Elementary Climate Physics*. Oxford University Press, 2005.